

ARTICLE

Population collapse and adaptive rescue during long-term chemostat fermentation

Navneet Rai^{1,2}  | Linh Huynh^{1,2} | Minseung Kim^{1,2} | Ilias Tagkopoulos^{1,2}¹UC Davis Genome Center, University of California, Davis, California²Department of Computer Science, University of California, Davis, California**Correspondence**Ilias Tagkopoulos, UC Davis Genome Center, University of California, Davis, CA 95616.
Email: itagkopoulos@ucdavis.edu**Funding information**

Army Research Office, Grant/Award Number: W911NF1210231; National Science Foundation, Grant/Award Numbers: 1516695, 1254205

Abstract

Microbial fermentation is an essential process for research and industrial applications, yet our understanding of cellular dynamics during long-term fermentation is limited. Here, we report a reproducible phenomenon of abrupt population collapse followed by a rapid population rescue that was observed during long-term chemostat cultivations, for various strains of *Escherichia coli* in minimal media. Through genome resequencing and whole-genome transcriptional profiling of replicate runs over time, we identified that changes in the tRNA and carbon catabolic genes are the genetic basis of this phenomenon. Since current fermentation models are unable to capture the observed dynamics, we present an extended model that takes into account critical biological processes during fermentation, and we further validated carbon source predictions through forward experimentation. This study extends the predictability of current models for microbial fermentation and adds to our system-level knowledge of cellular adaptation during this crucial biotechnological process.

KEYWORDS

cell elongation, fermentation, microbial evolution, transcriptomics, whole genome sequencing

1 | INTRODUCTION

Bacteria live in dynamic environments and have evolved a plethora of strategies, such as growth stagnation (Fridman, Goldberg, Ronin, Shores, & Balaban, 2014; Rai, Rai, & Venkatesh, 2015) and genetic modifications (Toprak et al., 2012) to cope with environmental variation (Denamur & Matic, 2006; Elena & Lenski, 2003; Feng, Lampel, Karch, & Whittam, 1998). These strategies emerge through evolutionary processes, such as random drift, natural selection, and horizontal gene transfer (Mozhayskiy & Tagkopoulos, 2012; Ochman, Lawrence, & Groisman, 2000) and are manifested through mutations in coding sequences (Toprak et al., 2012) or gene amplification (Blount, Barrick, Davidson, & Lenski, 2012; Dragosits, Mozhayskiy, Quinones-Soto, Park, & Tagkopoulos, 2013). Permanent genetic changes may give rise to strains with redesigned gene regulatory networks (Taylor et al., 2015) and other interesting traits, such as increased protein activities (Glieder, Farinas, & Arnold, 2002; Hoels et al., 2015). In stressful environments, organisms exhibit a rich repertoire of responses that are either due to direct physical and chemical effects to cellular proteins (Guo & Gross, 2014), DNA (Lopez-Garcia & Forterre, 2000), structural molecules (Raivio, 2005) and other compounds within

the cell (Ye et al., 2012), or part of an elaborate response program that initiates and often tightly regulated (Tan & Ramamurthi, 2014). Early on, this is manifested with a drop in growth rate, phenotypic and physiological changes (Barria, Malecki, & Arraiano, 2013; Mañas & Mackey, 2004), and later on through the fixation of adaptive mutations, which emerge in times scales that range from hours to days, depending on the type and the magnitude of the selection pressure (Good, McDonald, Barrick, Lenski, & Desai, 2017; Zhang et al., 2011; Zorraquino, Kim, Rai, & Tagkopoulos, 2017). Bacteria devise several strategies, such as developing persistence, inducing biofilm formation and making permanent changes in the genome, to rescue themselves, when encounter stressful environments. For example, in a genetically homogeneous microbial population, a fraction of cells, when encounter the antimicrobial, become metabolically dormant and stop the growth. These cells are called persister cells and when antimicrobials are removed from the environment, these cells resume the growth (Jöers, Kaldalu, & Tenson, 2010; Wood, Knabel, & Kwan, 2013). Alternatively, several bacteria, under sublethal antibiotic concentration, induce the cellular machinery responsible for the formation of thicker biofilm, making them more tolerant (Fux, Costerton, Stewart, & Stoodley, 2005). If the

environmental stress persists for longer duration, bacteria make permanent genetic changes to rescue themselves (Zorraquino et al., 2017).

Studies of bacterial evolution have mostly been performed under batch culture conditions in shake flasks or 96-well plates, which are cost-effective, easy to operate and do not require special instrumental setup. The batch and fed-batch environments can be particularly dynamic and difficult to model due to the large number of parameters involved. In addition to serial dilutions as a method used to study the adaptation and evolution of bacterial cultures (Blount et al., 2012; Zorraquino et al., 2017), chemostats have been used for evolutionary studies when controllability, reproducibility, and continuous growth in a well-controlled static or dynamic conditions is critical (Gresham & Hong, 2015; Hoskisson & Hobbs, 2005). Industrial applications of bacterial biofermentation in batch, fed-batch, and chemostat cultures are many and their value in the billions of dollars per year (Rossouw & Bauer, 2009; Selvamani, Friehs, & Flaschel, 2014; Vaiphei, Pandey, & Mukherjee, 2009). In industrial processes, the product yield, quality, and cost are influenced by the interactions between media components and the host strain (Gudiña, Teixeira, 2011; Hahn-Hägerdal et al., 2005). Despite their importance in both industrial and research applications, there are critical knowledge gaps when it comes to the comprehensive understanding of the molecular basis of long-term chemostat fermentation. Concomitantly, the current computational models are unable to capture the complex nonlinear dynamics that take place in such environments, hence constraining our options to a trial-and-error approach. As such, creating an accurate computational model that can generalize its predictions in novel environments is one of the grand challenges in computational biotechnology (Carrera et al. 2014; Kim et al. 2016; Kim and Tagkopoulos 2018; Kim et al. 2015; Mozhayskiy and Tagkopoulos 2013; Wang et al. 2018).

In an effort to bridge this gap, we systematically exposed *E. coli* strains in different media compositions under a chemostat environment

for 15–20 days (between 36 and 49 volume changes at dilution rate (D) = 0.1 hr⁻¹). Then we mapped the genome-wide transcriptional, genetic, and phenotypic changes of these cells, in an effort to understand both the processes and stages of phenotypic adaptation in a constant flow dynamic environment. We used these data sets to train extended mechanistic models to describe observed phenotypes and guide experimentation in uncharted experimental spaces (Figure 1). Interestingly, we recorded several reproducible phenomena including cell size elongation and an unexpected dynamic peak-valley cell density profile, a newly described phenomenon that we will refer to as stress-and-rescue. Whole genome resequencing was performed to investigate genotypic changes and RNA-Seq was used to identify differentially expressed genes (DEGs) at focal points during the course of the experiment.

2 | MATERIALS AND METHODS

2.1 | Strains and media

Evolutionary studies were performed with *E. coli* strains MG1655, HG105 (Garcia & Phillips, 2011), and BW25113 (Baba et al., 2006). For short-term preservation, cells were maintained on Luria Bertani (LB) agar plates and stored at 4°C. When required, a single colony was inoculated in LB broth and grown at 30°C in an incubator shaker (Innova 4230; New Brunswick Scientific, Edison, NJ) operating at 200 rpm. Long-run evolution studies were either done in LB broth or M9 media (Sambrook et al., 2001) supplemented with 0.2% casamino acids, 1 mM thiamine hydrochloride, and either glucose or glycerol as a carbon source.

2.2 | Chemostat and long-run evolution

A single colony of required *E. coli* strain was inoculated in 5 ml LB for 8 hr at 30°C in an incubator shaker and subsequently transferred to 100 ml of seed media. Seed medium was either LB or M9 salt media containing

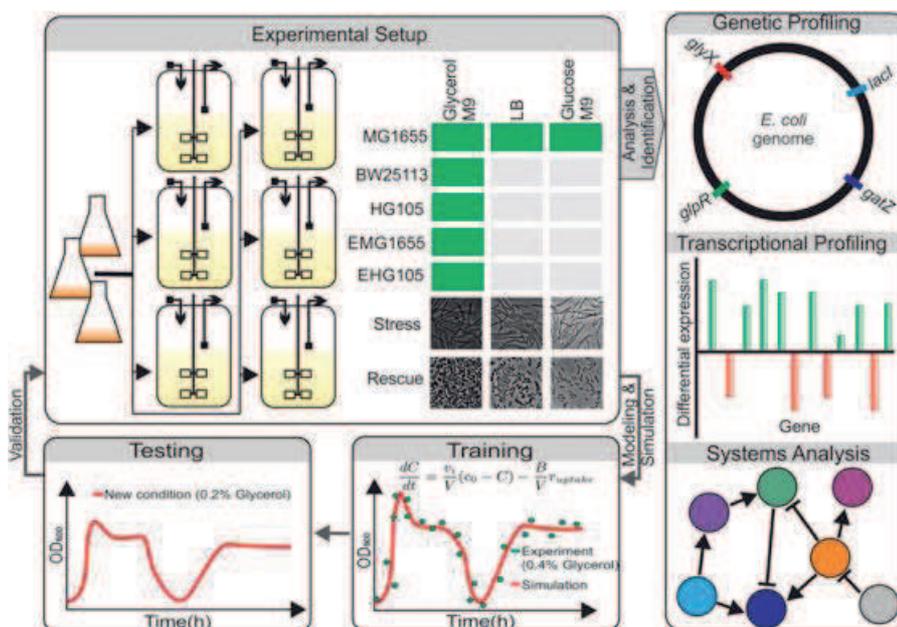


FIGURE 1 Overview of the experimental setting and computational approaches. Seed cultures of different strains of *E. coli* were prepared and then transferred to six parallel 1 L chemostats. Dilution rate was maintained at 0.1 hr⁻¹. Cells were harvested at desired time points for cell density, cell size, genetic, and transcriptional profiling. The computational model was developed and trained to capture the dynamics of cell density and subsequently predictions were experimentally validated [Color figure can be viewed at wileyonlinelibrary.com]

either glucose or glycerol. Seed culture was grown overnight at 30°C in an incubator shaker. Following day, fermenter vessel (Biostat Q+; Sartorius Stedim, Goettingen, Germany) containing 900 ml of required sterile media was inoculated with the seed culture, and chemostat was started at $D=0.1\text{ hr}^{-1}$. Operating volume of the chemostat was maintained at 1 L using two peristaltic pumps (Master Flex; L/S, Cole-Parmer, Vernon Hills, IL). Dissolved oxygen was maintained above 40%, temperature at 30°C, agitation at 600 rpm, pH was kept constant at 7.0 by adding 2 M NaOH, and antifoam (Antifoam 204; Sigma, St. Louis, MO) was added automatically when required. Cells were harvested from the chemostat at the required time points.

2.3 | Whole genome resequencing

Cells from 1 ml of culture growing in 0.4% glycerol M9 chemostat were harvested at the specified time points. Cells were pelleted down at 13,200 rpm at room temperature and stored at -80°C until use. Genomic DNA (gDNA) was isolated using a Wizard Genomic DNA Purification Kit (Promega, Madison, WI). Integrity of gDNA was checked on 0.8% agarose gel. Concentrations of gDNA were measured using NanoDrop (Thermo Scientific, Waltham, MA). For the library preparation, approximately 5 μg of gDNA was fragmented in a bioruptor (Diagenode, Denville, NJ) sonication apparatus. Libraries from fragmented DNA were prepared using KAPA Library Preparation Kit (Kapa Biosystems, Wilmington, MA). Size selections of libraries were performed using Agencourt AMPure XP (Beckman Coulter, Brea, CA). Quality of individual library was checked on Bioanalyzer (Agilent Technologies, Santa Clara, CA), and subsequently libraries were pooled together and sequenced at Illumina HiSeq. 2500 platform running in high throughput mode (Paired end, 100 cycles). Based on the pre-designed barcodes, the fastQ file generated by the machine was demultiplexed into individual file corresponding each gDNA sample (see Supporting Information Methods for the details of analysis).

2.4 | Gene expression analyses

Cells growing in 0.4% glycerol M9 chemostat were harvested at 72, 150 and 300 hr. At defined time points, 1 ml of growing culture was mixed with chilled 0.5 ml 5% phenol/ethanol (vol/vol), and cells were pelleted down at 13,200 rpm at 4°C. Cell pellets were stored immediately at -80°C until use. RNA was extracted using a RNeasy kit (Qiagen, Hilden, Germany). Quality of RNA was checked on 1.5% denaturing agarose gel. mRNA enrichment was performed using Bacterial mRNA Enrichment Kit (Thermo Scientific, Waltham, MA). Libraries from mRNA enriched samples were prepared using Kapa standard RNA-Seq library preparation kit (Kapa Biosystems, Wilmington, MA). Double size selections of the libraries were performed using Agencourt AMPure XP (Beckman Coulter, Brea, CA). Quality of individual library was checked on Bioanalyzer (Agilent Technologies, Santa Clara, CA). All libraries were pooled together and sequenced by Illumina HiSeq. 2500 running in high throughput mode (single end, 50 cycles). DEGs common between 150 and 300 hr were also analyzed and functional annotation was performed using the GSEA software (Subramanian et al., 2005). GSEA gene sets used were

downloaded from bioinformatics.org/go2msg (gene sets used can be provided upon request). Minimum lengths of the RNA-Seq libraries were 200 bp, so most of the tRNA, which are less than 100 nucleotide long (Sharp, Schaack, Cooley, Burke, & Soil, 1985), will be lost during fragmentation and size selection steps of the library preparation, hence tRNAs were excluded in the analysis. See Supporting Information Methods for the RNA-Seq data analysis and DEG analysis.

2.5 | Growth rate measurements

A single colony each of ancestor and evolved MG1655 strains were inoculated separately in 1 ml LB broth and grown overnight at 30°C in an incubator shaker operating at 200 rpm. Following day, 3 μl of the growing cultures were taken and inoculated into 197 μl of 0.4% glycerol M9 media in a 96-well flat-bottom plate (Costar, Kennebunk, ME). Growth profiles were measured in a plate reader (BioTek Synergy HT, Winooski, VT) operating at 30°C. Cell densities were measured every 15 min at 600 nm wavelength. Growth rates were calculated using an automated script in the MATLAB. Growth rates were determined by calculating the differential between 10% and 90% of cell density using a virtual sliding window with a width of 1 hr and sliding every 15 min. For each growth profile, highest value of differential was considered as maximum growth rate.

2.6 | Phase contrast imaging and cell size measurement

One milliliter culture was taken, and cells were pelleted down by centrifugation at 10,000 rpm for 5 min. Pellets were dissolved in an appropriate volume of M9 salt medium. Five microliters of *E. coli* suspension was placed on a microscope slide (Corning, NY) and pressed gently under a coverslip to fix the cells. 100X phase contrast images were taken using Axio Lab.A1 (Zeiss, Oberkochen, Germany) microscope. Length of 100 *E. coli* cells were measured at 0 and $152.67 \pm 8.67\text{ hr}$ using ImageJ (imagej.nih.gov/ij/). Subsequently, mean cell-length and standard error of mean were calculated by the OriginPro statistical analysis software (OriginLab Corporation).

2.7 | Computational simulation

We used MATLAB to simulate the model. All the code, initial conditions, and a walkthrough on how to reproduce the simulation results are publicly available at <https://ibpa.github.io/ChemostatModel>

3 | RESULTS AND DISCUSSION

3.1 | Reproducible stress-and-rescue phenomenon in long-term chemostat settings

Parallel chemostats with 0.4% glycerol M9 minimal media operating at 30°C were established. In this setting, growth profiles of *E. coli* MG1655 cultures were measured up to $360.3 \pm 11.7\text{ hr}$ in biological triplicates. D was maintained at 0.1 hr^{-1} and pH was maintained at

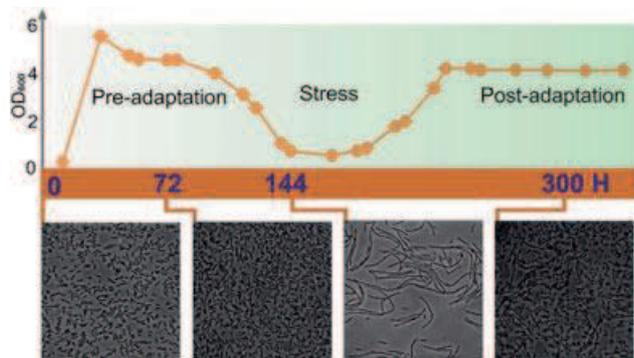


FIGURE 2 Growth profile and cell size dynamics of *Escherichia coli* MG1655 in a 0.4% glycerol M9 chemostat at 30°C. The population overshoots, then stabilizes between 48 to 72 hr. After 72 hr, population starts collapsing which is rescued at 150 h by adaptive mutations and finally stabilizes at an optical density (OD) of 4 around 250 hr. For each condition, chemostats were performed in triplicate. At desired time points, samples from each chemostat were drawn three times to measure the technical errors. OD values are given as the mean \pm SEM ($n = 3$; technical replicates) [Color figure can be viewed at wileyonlinelibrary.com]

7.0 by automatically adding 2 M NaOH. We observed that each chemostat culture achieves steady state cell density at 48 hr and maintains it for 77 ± 2.85 hr (Figure 2 and Supporting Information S1A). After 77 ± 2.85 hr the chemostat destabilizes and the cell density decreases with an exponential rate to an optical density (OD)₆₀₀ of 0.55 ± 0.06 at 152.67 ± 8.67 hr. Interestingly, the chemostat cultures maintain an OD₆₀₀ close to 0.6 ± 0.07 for 33.67 ± 4.41 hr and then cell density increases until it regains a steady state OD₆₀₀ of 4.35 ± 0.35 . Once this occurs, it maintains that cell density until the completion of the experiment. This phenomenon was observed in all glycerol M9 chemostat cultures we administered in this study. We observed that the *E. coli* cells elongated substantially with the progression of the chemostat, with a maximum elongation at 152.67 ± 8.67 hr. The average cell diameter at 0 hr was observed to be 2.8 ± 0.14 μm and at 152.67 ± 8.67 hr, it was nine-fold larger at 23.4 ± 1.5 μm . Interestingly, cell size reverts to normal as cell density increases and then maintains normal values until the end of the

experiments (360.3 ± 11.7 hr). This phenomenon is not limited to the MG1655 strain, as we reproduced it with all strains tested, including the HG105 (Garcia & Phillips, 2011) and BW25113 (Baba et al., 2006) strains (Figure 3a, Supporting Information S1B and S2).

Further experiments were performed to measure the dependency of the observed drop in cell density on the media composition. *E. coli* MG1655 cells were grown in M9 salt chemostats supplemented with glucose, and in LB broth, separately (Supporting Information Figure S1C and D). This phenomenon was only observed in the chemostats with the minimal M9 media, hence, there is a dependency between the stability of steady state cell density and the growth medium composition. To find out, if evolution in 0.4% glycerol M9 media provides any growth fitness, growth measurements were performed in a plate reader. It was observed that the evolved MG1655 population was growing significantly faster than the wild-type MG1655 (Supporting Information Figure S4).

Next, we investigated whether the rescued cells had acquired genetic changes that protect them from the stagnation in growth if the experiment was to be repeated. To test this hypothesis, evolved MG1655 and HG105 cells from the terminal time points of the glycerol chemostat were harvested and spread on LB agar plates. Colonies from these fresh plates were picked-up and glycerol M9 chemostats at 30°C were initialized with the same conditions as previously. Interestingly, these evolved cells maintained the normal steady state cell density and cell size throughout the experiment (Figure 3b, Supporting Information S3), suggesting that permanent genetic changes are responsible for this adaptation. Growth rates of the wild-type and evolved strains were also measured in 0.4% glycerol M9 at 30°C in a plate reader. In all cases, the evolved MG1655 outperformed the growth rate of ancestral wild-type MG1655 strain by $52.8\% \pm 21.4\%$.

3.2 | Transcriptional and ontology analysis

Transcriptional profiling was performed to identify changes in biological processes before, during and after cell adaptation. Cells were harvested at three time points corresponding to the pre-adaptation steady state (72 hr), the lowest OD state (150 hr),

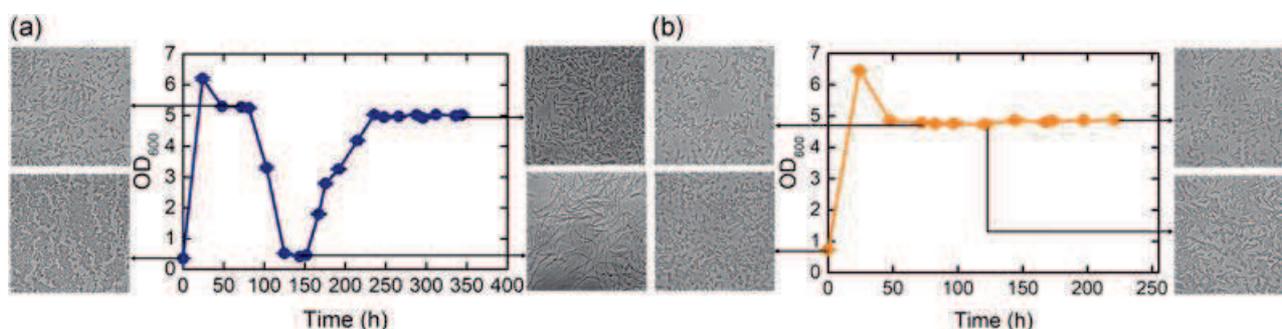


FIGURE 3 Growth profiles and cell size dynamics of wild-type and evolved *Escherichia coli* strains in a 0.4% glycerol M9 chemostat operation at 30°C. (a) Growth profiles and cell size dynamics of wild-type HG105. (b) Growth profiles and cell size dynamics of evolved MG1655. Population collapse is observed in wild type but not in evolved cell populations. Optical density (OD) values are given as the mean \pm SEM ($n = 3$; technical replicates) [Color figure can be viewed at wileyonlinelibrary.com]

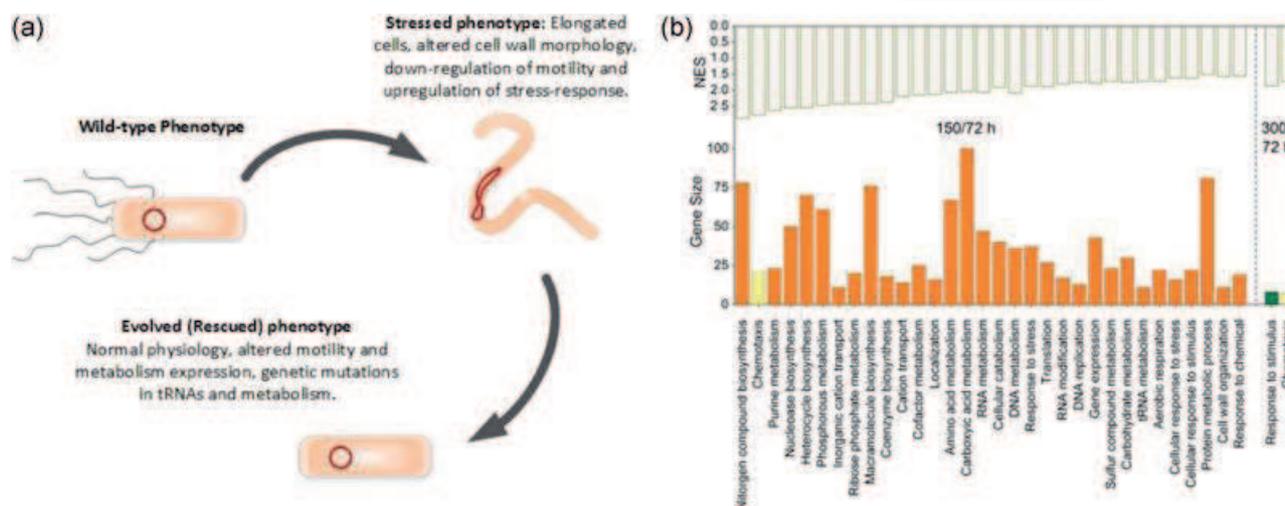


FIGURE 4 Stress-and-rescue progression and differential pathway analysis. (a) The progression of the stress-and-rescue phenomenon. (b) Cellular components and processes that were found significantly affected based on the Normalized Enrichment Score (NES) 150 and 300 hr in 0.4% glycerol M9 chemostat, with respect to the 72 hr time point (control). Genes involved in the chemotaxis were significantly affected at both the 150 and 300 hr time points [Color figure can be viewed at wileyonlinelibrary.com]

and the adapted state (300 hr). Compared with 72 hr, 1233 and 33 genes were differentially expressed (fold change > 2) at 150 hr and at 300 hr, respectively (Figure 4). Interestingly, 21 of the 33 DEGs exist both in 150 and 300 hr, corresponding to bacterial motility and response to stimulus (Dragosits et al., 2013; Franchini & Egli, 2006; López-Maury, Marguerat, & Bähler, 2008).

In agreement with our microscopy observations, cell growth, cell wall and cell membrane genes were differentially expressed (Figure 4; Supporting Information Table S1; see DEGs clustering by GSEA in Supporting Information Material), as they play a major role during stress adaptation (Atsumi et al., 2010; Dragosits et al., 2013; Sandberg et al., 2014). Similarly, bacterial motility genes were also found to be perturbed and downregulated (Maurer, Yohannes, Bondurant, Radmacher, & Slonczewski, 2005). Glycerol metabolism genes, such as *glpQ* and *glpD* were also upregulated. Interestingly, genes *gnsA*, *sulA*, and *dinD*, which are involved directly or indirectly with the cell elongation, were induced at the 150 hr (Huisman, D'Ari, & Gottesman, 1984; Ohmori et al., 1995; Sugai, Shimizu, Nishiyama, & Tokuda, 2004). As expected, numerous genes related to stress response were differentially expressed. *sulA*, a SOS response-related gene is upregulated at the 150 hr (McKenzie, Harris, Lee, & Rosenberg, 2000). SulA binds to and inhibits the assembly of FtsZ by a simple sequestration method (Chen, Milam, & Erickson, 2012). FtsZ is a bacterial cytoskeletal protein involved in the cell division, and it has been reported that *E. coli* cells with low levels of FtsZ form filaments, which is in agreement with our phenotypic characterization with microscopy (Dai & Lutkenhaus, 1991). Other SOS responsive genes such as *recA*, *dinD*, and *dinF* were also upregulated. The *dnaK* and *dnaJ* genes, which encode the HSP70 heat shock response system, were also induced. The *mazG* gene, which encodes a nucleoside pyrophosphohydrolyase hydrolyzing noncanonical dNTPs, was also induced. Induced level of MazG helps cells survive under nutritional stress and also inhibits the growth rate (Gross, Mar-

ianovsky, & Glaser, 2006), which could be contributing to the loss in cell density observed at 150 hr. Notably, enzymatic activity of MazG is inhibited by an elevated level of MazEF (Gross et al., 2006), but in our experiments, MazEF was not activated at 150 hr, hence MazG was fully active. Other stress-protecting genes such as *oppA* (differential codon utilization) and *cpxP* (resistance to pH stress) were also overexpressed.

3.3 | The genetic basis of adaptation to long-term chemostat cultures

Whole genome resequencing of the *E. coli* MG1655 cells collected at representative time points during the chemostat cultivation (samples at 0, 72, 150, and 300 hr; Figure 5) was performed to explore the genetic basis of adaptation. Resequencing analysis showed that biological replicates of *E. coli* MG1655 were following a parallel evolution path in the chemostat.

3.3.1 | Biomodal growth and glycerol metabolism

Figure 5 depicts the mutations which were emerged at different time points. From the target genes, *glpR* and *gatZ* are associated with the glycerol metabolism (Lin, 1976; Tran, Maeda, Sanchez-Torres, & Wood, 2015). *GlpR* is the repressor of sn-glycerol-3-phosphate regulon which is composed of several operons (Schweizer, Boos & Larson, 1985; Yang, Gerhardt, & Larson, 1997) responsible for the metabolism of glycerol and glycerol-3-phosphate. Interestingly, a recent study demonstrated that when *Pseudomonas putida* is grown in glycerol supplemented growth media, it showed bimodal growth/no-growth patterns, with *GlpR* responsible for bimodal growth (Nikel, Romero-Campero, Zeidman, Goñi-Moreno, & de Lorenzo, 2015). The second gene *gatZ* is a member of the *gat* operon driving the galactitol metabolism (Nobelmann & Lengeler, 1996). *GatZ* is a component of

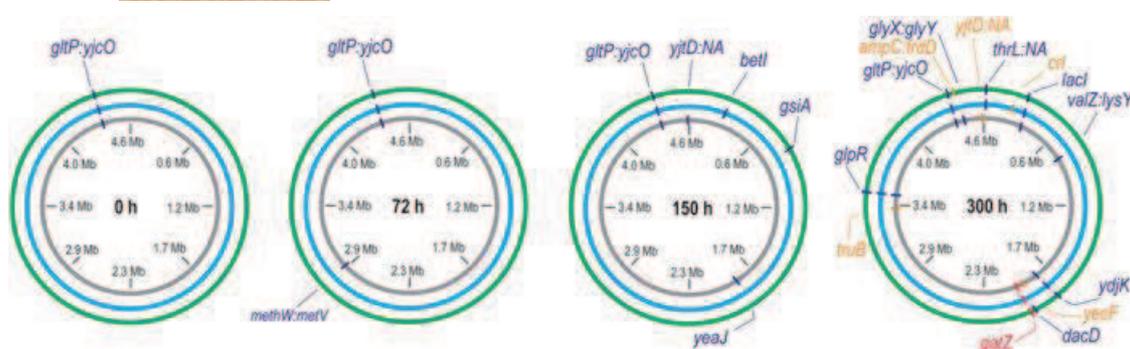


FIGURE 5 Whole genome resequencing of MG1655 at four different time points. *Escherichia coli* MG1655 cells from the three 0.4% glycerol M9 chemostat replicate populations were collected at four time points (0, 72, 150, and 300 hr) for the resequencing. Layers in the circles represent the biological replicates. Mutations were marked with different colors for clarity at 300 hr [Color figure can be viewed at wileyonlinelibrary.com]

tagatose-bisphosphate aldolase, which catalyzes a reversible reaction D -tagatofuranose 1,6-bisphosphate glycerone phosphate + D -glycer-aldehyde 3-phosphate. In presence of glycerol, GatZ can divert glycerol catabolism products glycerone phosphate and D -glyceraldehyde 3-phosphate to the synthesis of D -tagatofuranose 1,6-bisphosphate, which is likely to result in growth inhibition. Thus, inhibition of GatZ in a glycerol-based chemostat leads to rapid growth after rescue, in agreement with recent observations (Tran et al., 2015).

3.3.2 | Sigma factors and general stress response

One of the evolved strains had a mutation in *crl*. Crl is a thermosensor with maximum concentration during the stationary phase at 30°C (Bougourd, Lelong, & Geiselmann, 2004). Crl interacts with one of the seven *E. coli* sigma factors (σ), and enhances the transcription of general stress responsive regulon (Banta et al., 2013). The complex of sigma factor and RNA polymerase core enzyme initiates the transcription, and each sigma factor interacts with a specific group of promoters (Österberg, Peso-Santos, & Shingler, 2011). Furthermore, several independent studies have also reported that *E. coli* with mutations in *crl* demonstrated an improved growth rate (Bougourd et al., 2004; Madan, Moorthy, & Mahadevan, 2008).

3.3.3 | Gene regulation through tRNAs

Finally, several mutations were mapped in the intergenic regions of tRNA encoding genes (see Table S2 in Supporting Information Material). Several independent studies have demonstrated that cellular tRNA pool might dynamically change upon stress to support the efficient translation of adaptive genes (Torrent, Chalancon, de Groot, Wuster, & Madan Babu, 2018; Yona et al., 2013; Zhong et al., 2015), and that mutations in intergenic regions influence the expression of upstream and downstream genes (Sandberg et al., 2014). Further studies are required to identify the exact mechanism, including hypotheses related to the fact that intergenic regions of *E. coli* contain multiple small untranslated RNAs which regulate expression of target genes such as iron storage and iron-using genes in iron limited environment (Argaman et al., 2001; Massé & Gottesman,

2002). Several other interesting mutations appeared in the resequenced genome (Figure 5, Supporting Information Table S2).

3.4 | Predictive model of chemostat cultures

To better understand the dynamics of a long-term chemostat culture, we built a mathematical model based on a model by Herbert et al. model (Herbert, Elsworth, & Telling, 1956) and first principles governing growth (see Supporting Information Methods). However, this basic model cannot explain the observed behavior and data collected, due to the limitations (see Supporting Information Table S3 and Figure S5). To address them, we introduce an extended model (see Supporting Information Table S3) including the following extensions:

- Modeling the “overshoot” effect: Let K_M and K_C be two constants that represent the dependence of the growth rate and the carbon source uptake rate on the carbon source concentration (see Equations 2 and 4 in Supporting Information Methods). We simulated different values of K_M and K_C (Supporting Information Figure S6) to understand when overshooting appears in the first few hours of growth. The “overshooting” effect can be captured when $K_M > K_C$. Therefore, let $\alpha = K_M/K_C > 1$, the growth rate formula of Herbert et al model (see Equation (4) in Supporting Information Methods) can be rewritten as

$$\mu = \mu_{\max} \frac{C}{C + \alpha K_C}. \quad (1)$$

Here, μ , μ_{\max} , and C are the growth rate, the maximum growth rate, and the carbon source concentration, respectively (see Supporting Information Table S4).

- Nonlinear OD-to-carbon mapping: Some factors (e.g. acetate) inhibit growth when the cell density increases (Shiloach & Fass, 2005). As such, the available carbon sources per cell will be decreased, because of higher cell density and the efflux. Here, we tried using a polynomial function and a Hill function to take this dependence into account. We observed that the polynomial

function gave a better prediction than the Hill function (see Supporting Information Figure S7). Therefore, the equation that describes the carbon source change in Herbert et al model (see equation 1 in Supporting Information Methods) can be reformulated as:

$$\frac{dC}{dt} = \frac{v_i}{V}(c_0 - C) - \frac{B}{V}r_{\text{uptake}} \times \left(1 + \left(\frac{B}{K_B}\right)^{n_B}\right), \quad (2)$$

where C and B are the carbon source concentration and the biomass respectively, r_{uptake} is the maximum carbon source uptake rate, V , v_i , and c_0 are the volume, influx-rate, and the influx carbon source concentration respectively, and K_B and n_B are parameters of the polynomial function (see Supporting Information Table S4).

- OD drop: Since the stress-and-rescue phenomenon only appeared in the minimum medium M9 but not in the rich medium LB (see Supporting Information Figure S1), we hypothesized that the stress was from the nutrient limitation. Therefore, the stress should be modeled as a function of multiple variables including the cell density, the glycerol, and the time. However, we observed that:

- (1) There was a long time period (25 hr, from 55 hr to 80 hr, Figure 2) when the OD was stable. Therefore, the glycerol concentration was also stable in this period. However, the OD only dropped at the end of this period. This implied that the stress did not appear and affect the growth rate immediately due to the change in the cell density or the glycerol concentration. Rather, there was a delay between the time point the stress appeared to the time point the stress affected the growth rate. Thus, neither the glycerol concentration alone nor the cell density alone is predictive for the stress.
- (2) After the OD dropped, there was a long time period (10 hr, from 150 hr to 160 hr, Figure 2) when the glycerol was abundant (since OD was very low, the consumption should be very small) but the cell could not escape the stress. This implied that the stress was not reversible by increasing the glycerol.
- (3) The time point when the OD dropped and the trend of the OD drop were quite similar in all four experiments (chemostats with 0.1%, 0.2%, 0.4%, 0.8% glycerol). It implied that the contribution of the glycerol concentration was negligible in predicting the stress and its effect on the growth rate.

Therefore, to satisfy (1) and (2), a complete model of the stress must be a complex function of both the glycerol concentration, the cell density and the time. However, considering the limited availability of experimental data and limited understanding about the impact of the stress to the environmental dynamics, it is not advisable to build a complicated model while the role of the glycerol concentration and the cell density is negligible. Therefore, we modeled the stress by an empirical function of time only. More specifically, the M9 medium does not provide required

nutrients for the balanced growth, resulting in cell stress, which in turn reduces growth after a given delay T_0 . We used a sigmoid function with a slope β to calculate the stress coefficient, a quantity that is a function of time and can be thought as a weight or probability:

$$\text{Stress} = \frac{1}{1 + e^{\beta(T_0 - t)}}. \quad (3)$$

Overall, the growth rate (Equation 1) is extended by factoring in its relationship to the growth inhibition, the cell density stress coefficient:

$$\mu = \mu_{\text{max}} \frac{C}{C + \alpha K_C} \times (1 - \text{Stress}). \quad (4)$$

In all experiments, we manually set the delay $T_0 = 115$.

- OD increase: After the OD drops, it appears that a fraction of mutant cells grow and take over the stressed and nondividing cells. As a result, OD starts increasing again and achieves the steady state. We assume that the wild-type (WT) cells and the mutant cells share the same function form of up-taking carbon source and growing (Equations 5-8), but the parameter values of these

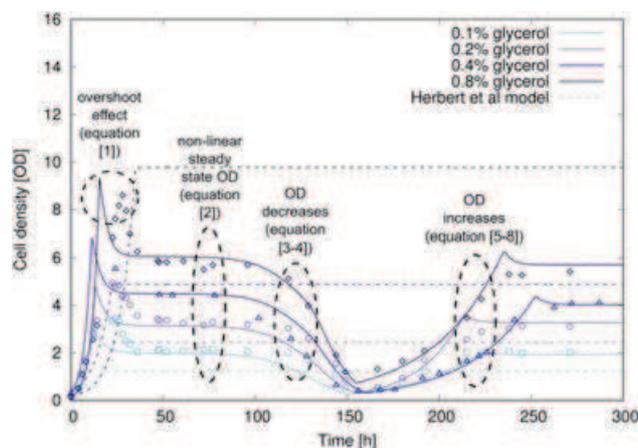


FIGURE 6 Model dynamics of chemostat cultivation for different carbon source concentrations. Data from the 0.2% and 0.4% glycerol run were used to make forward predictions for the 0.1% and 0.8% glycerol cultures. The model simulations (continuous lines) and experimental data (points) exhibit similar dynamics that match the change in carbon source concentration in general. Dotted lines correspond to the basic model by Herbert et al. (1956). For 0.1% glycerol, PCC and RSS/SS of the extended model are 0.89 and 7.7/119 while the ones of Herbert model are 0.51 and 39.4/119. For 0.8% glycerol, PCC and RSS/SS of the extended model are 0.91 and 28.3/695.6, while the ones of Herbert model are 0.34 and 421/695.6. All these PCCs and ratios are calculated from the predicted ODs and experimental ODs of the wild-type strain growth (0–150 hr). OD: Optical density; PCC: Pearson correlation coefficients; RSS: residual sum of squares; SS: sum of squares [Color figure can be viewed at wileyonlinelibrary.com]

TABLE 1 Overview of the selected potential mutations observed in *Escherichia coli* MG1655 in 0.4% glycerol M9 chemostat at 30°C, which could play significant role in the adaptation

Genes	Pathway	Effect		Novel	References
		Wild-type	Mutant		
<i>gatZ</i>	Galactitol degradation	Slower growth	Higher growth	No	Nobelmann and Lengeler (1996), Tran et al. (2015)
<i>glpR</i>	Glycerol metabolism	Bimodal growth	Normal growth	Yes ^a	Lin (1976), Nickel et al. (2015)
<i>crL</i>	Transcription	σ^S inducer, lower growth	Higher growth	No	Banta et al. (2013), Bougdour et al. (2004), Madan et al. (2008)
<i>tRNA (intergenic region)</i>	Translation	Normal translation	Adapted translation	No	Yona et al. (2013)

^aReported in *Pseudomonas putida*.

functions are different for each strain (i.e. r_{\max} , μ_{\max} , α). To simulate the cell growth in an experiment, we divided the simulation into two periods. In the first period (before the mutants appeared), the parameter values of the WT can be described as

$$r_{\text{uptake}} = r_{\max}^{\text{WT}} \frac{C}{C + K_C}, \quad (5)$$

$$\mu = \mu_{\max}^{\text{WT}} \frac{C}{C + \alpha^{\text{WT}} K_C}. \quad (6)$$

In the second period (after the mutants appeared), the parameter values of the mutant can be described as

$$r_{\text{uptake}} = r_{\max}^{\text{mutant}} \frac{C}{C + K_C}, \quad (7)$$

$$\mu = \mu_{\max}^{\text{mutant}} \frac{C}{C + \alpha^{\text{mutant}} K_C}. \quad (8)$$

Our current model cannot predict when the mutant population will appear. Instead, the appearance of the adapted mutant was set manually in our simulations at 150, 155, 160, and 155 hr for the experiment with 0.1%, 0.2%, 0.4%, and 0.8% glycerol, respectively. These time points were also used to divide the simulation into two periods for each experiment.

Since the wild-type strain was same in all four experiments (i.e. with different glycerol concentrations), the model parameter values of the wild-type could be estimated by fitting the model with experimental data of different experiments simultaneously. In contrast, the mutant strain may be different in each experiment. Given no other information, it is not possible to predict the growth dynamics of adapted mutant cells, hence to capture these dynamics, we had to train the model on each experiment separately. As a result, four parameter value combinations were estimated where each one was for the mutant of one experiment. These four parameter value combinations and one of the wild-types were shown in Supporting Information Table S4.

Data from 0.2% and 0.4% glycerol experiments were used to make forward predictions for the 0.1% and 0.8% glycerol cultures. The simulation of our extended model can capture the experi-

mental data (Figure 6) for 0.2% glycerol and 0.4% glycerol. Most importantly, the extended model gave a better prediction of the wild-type strain growth (0–150 hr) than Herbert model did for 0.1% and 0.8% glycerol experiment. Specifically, we evaluated the prediction by the Pearson correlation coefficients (PCCs) between the predicted ODs and the experimental ODs. PCCs of the extended model were 0.89 and 0.91 for experiments with 0.1% glycerol and 0.8% glycerol, respectively, while these PCCs of Herbert model were only 0.51 and 0.34. In addition, we evaluated the prediction by the ratio between the residual sum of squares (RSS; between predicted ODs and experimental ODs) over the sum of squares (SS) of experimental ODs. These ratios of the extended model were 7.7/119 and 28.3/695.6 for experiments with 0.1% glycerol and 0.8% glycerol, respectively, while these ratios of Herbert model were 39.4/119 and 421/695.6.

4 | CONCLUSION

This study describes a stress-and-rescue phenomenon where *E. coli* populations cease growth under stress, cells dramatically change their phenotype by becoming filamentous, and the population collapses only to be rescued by genetic modifications (Table 1) and alternative expression patterns. Observed mutations are likely to be random and may even pre-exist in the population at low frequencies, and then are fixed once the selection pressure makes them adaptive (Galhardo, Hastings, & Rosenberg, 2007; Roy, 2016; Wrande, Roth, & Hughes, 2008).

The phenomenon is reproducible and occurs for different strains in minimal media. We expect this phenomenon exists due to the fact that some essential metals are not available in minimal medium cultures, as we do not see this phenomenon in rich media such as LB broth. We systematically dissected this phenomenon by applying computational and experimental techniques, which led to an extended model of microbial chemostat fermentation, as well as identification of the genetic and transcriptional basis of this phenomenon.

Our results demonstrate that accurate mechanistic models to predict the experimental trajectory of a chemostat setting are within reach. We only experimented and validated the model with different levels of the

same carbon source in a constrained environment, so further work is needed if we aspire to produce truly predictive models that can be useful for guiding experimentation or building an industrial process at-scale. Still, this study presents a clear advance on this front and it can serve as the foundations for further extensions.

Aside from the apparent intellectual merit of presenting a previously undocumented phenomenon, this study argues both for the advantages and the limitations of chemostat fermentation. The fact that the biological replicate trajectories were particularly reproducible makes chemostats an asset in long-term fermentation processes, such as adaptive laboratory experimentation. The way the cells experience the stressful environment and escaped from it is an excellent example of cellular plasticity, the behavior they employ to cope with environmental variation and the mechanisms that exist for short-term (changes in expression) and long-term (genetic modifications) adaptation. Our results implicate genes related to biomodal growth, carbon metabolism, cell membrane organization, general stress response elements and tRNA regulatory modifications. This and other similar work add another piece of the microbial puzzle and brings us closer to understand, predict, and engineer these “endless forms most beautiful” of the microcosmos.

ACKNOWLEDGMENTS

This study was supported by ARO award W911NF1210231 and NSF awards 1254205 and 1516695 to IT. JaeSung Youn for helping in setting up the GitHub page.

CONFLICTS OF INTEREST

The authors declare that there are no conflicts of interest.

ORCID

Navneet Rai  <http://orcid.org/0000-0002-2321-2378>

REFERENCES

- Argaman, L., Hershberg, R., Vogel, J., Bejerano, G., Wagner, E. G. H., Margalit, H., & Altuvia, S. (2001). Novel small RNA-encoding genes in the intergenic regions of *Escherichia coli*. *Current Biology*, *11*(12), 941–950.
- Atsumi, S., Wu, T.-Y., Machado, I. M. P., Huang, W.-C., Chen, P.-Y., Pellegrini, M., & Liao, J. C. (2010). Evolution, genomic analysis, and reconstruction of isobutanol tolerance in *Escherichia coli*. *Molecular Systems Biology*, *6*(1), 449–449.
- Baba, T., Ara, T., Hasegawa, M., Takai, Y., Okumura, Y., Baba, M., ... Mori, H. (2006). Construction of *Escherichia coli* K-12 in-frame, single-gene knockout mutants: The Keio collection. *Molecular Systems Biology*, *2*, 1.
- Banta, A. B., Chumanov, R. S., Yuan, A. H., Lin, H., Campbell, E. A., Burgess, R. R., & Gourse, R. L. (2013). Key features of σ S required for specific recognition by Crl, a transcription factor promoting assembly of RNA polymerase holoenzyme. *Proceedings of the National Academy of Sciences*, *110*(40), 15955–15960.
- Barria, C., Malecki, M., & Arraiano, C. M. (2013). Bacterial adaptation to cold. *Microbiology*, *159*(Pt 12), 2437–2443.
- Blount, Z. D., Barrick, J. E., Davidson, C. J., & Lenski, R. E. (2012). Genomic analysis of a key innovation in an experimental *Escherichia coli* population. *Nature*, *489*(7417), 513–518.
- Bougdour, A., Lelong, C., & Geiselmann, J. (2004). Crl, a low temperature-induced protein in *Escherichia coli* that binds directly to the stationary phase σ subunit of RNA polymerase. *Journal of Biological Chemistry*, *279*(19), 19540–19550.
- Carrera, J., Estrela, R., Luo, J., Rai, N., Tsoukalas, A., Tagkopoulos, I. (2014). An integrative, multi-scale, genome-wide model reveals the phenotypic landscape of *Escherichia coli*. *Molecular Systems Biology*, *10*(7), 735.
- Chen, Y., Milam, S. L., & Erickson, H. P. (2012). SulA inhibits assembly of FtsZ by a simple sequestration mechanism. *Biochemistry*, *51*(14), 3100–3109.
- Dai, K., & Lutkenhaus, J. (1991). ftsZ is an essential cell division gene in *Escherichia coli*. *Journal of Bacteriology*, *173*(11), 3500–3506.
- Denamur, E., & Matic, I. (2006). Evolution of mutation rates in bacteria. *Molecular Microbiology*, *60*(4), 820–827.
- Dragosits, M., Mozhayskiy, V., Quinones-Soto, S., Park, J., & Tagkopoulos, I. (2013). Evolutionary potential, cross-stress behavior and the genetic basis of acquired stress resistance in *Escherichia coli*. *Molecular Systems Biology*, *9*(1), 643–643.
- Elena, S. F., & Lenski, R. E. (2003). Evolution experiments with microorganisms: The dynamics and genetic bases of adaptation. *Nature Reviews Genetics*, *4*(6), 457–469.
- Feng, P., Lampel, K. A., Karch, H., & Whittam, T. S. (1998). Genotypic and phenotypic changes in the emergence of *Escherichia coli* O157: H7. *Journal of Infectious Diseases*, *177*(6), 1750–1753.
- Franchini, A. G., & Egli, T. (2006). Global gene expression in *Escherichia coli* K-12 during short-term and long-term adaptation to glucose-limited continuous culture conditions. *Microbiology*, *152*(7), 2111–2127.
- Fridman, O., Goldberg, A., Ronin, I., Shoshitashvili, N., & Balaban, N. Q. (2014). Optimization of lag time underlies antibiotic tolerance in evolved bacterial populations. *Nature*, *513*(7518), 418–421.
- Fux, C. A., Costerton, J. W., Stewart, P. S., & Stoodley, P. (2005). Survival strategies of infectious biofilms. *Trends in Microbiology*, *13*(1), 34–40.
- Galhardo, R. S., Hastings, P. J., & Rosenberg, S. M. (2007). Mutation as a Stress Response and the Regulation of Evolvability. *Critical Reviews in Biochemistry and Molecular Biology*, *42*(5), 399–435.
- Garcia, H. G., & Phillips, R. (2011). Quantitative dissection of the simple repression input–output function. *Proceedings of the National Academy of Sciences*, *108*(29), 12173–12178.
- Glieder, A., Farinas, E. T., & Arnold, F. H. (2002). Laboratory evolution of a soluble, self-sufficient, highly active alkane hydroxylase. *Nature Biotechnology*, *20*(11), 1135–1139.
- Good, B. H., McDonald, M. J., Barrick, J. E., Lenski, R. E., & Desai, M. M. (2017). The dynamics of molecular evolution over 60,000 generations. *Nature*, *551*(7678), 45–50.
- Gresham, D., & Hong, J. (2015). The functional basis of adaptive evolution in chemostats. *FEMS Microbiology Reviews*, *39*(1), 2–16.
- Gross, M., Marianovsky, I., & Glaser, G. (2006). MazG—a regulator of programmed cell death in *Escherichia coli*. *Molecular Microbiology*, *59*(2), 590–601.
- Gudiña, E. J., Teixeira, J. A., Rodrigues, Lg. R., & Rodrigues, L. R. (2011). Biosurfactant-producing Lactobacilli: Screening, production profiles, and effect of medium composition. *Applied and Environmental Soil Science*, *2011*, 1–9.
- Guo, M. S., & Gross, C. A. (2014). Stress induced remodeling of the bacterial proteome. *Current Biology*, *24*(10), R424–R434.
- Hahn-Hägerdal, B., Karhumaa, K., Larsson, C. U., Gorwa-Grauslund, M., Görgens, J., & Van Zyl, W. H. (2005). Role of cultivation media in the development of yeast strains for large scale industrial use. *Microbial Cell Factories*, *4*(1), 31–31.

- Herbert, D., Elsworth, R., & Telling, R. C. (1956). The continuous culture of bacteria; a theoretical and experimental study. *Microbiology*, 14(3), 601–622.
- Hoesl, M. G., Oehm, S., Durkin, P., Darmon, E., Peil, L., Aerni, H.-R., ... Budisa, N. (2015). Chemical evolution of a bacterial proteome. *Angewandte Chemie International Edition*, 54(34), 10030–10034.
- Hoskisson, P. A., & Hobbs, G. (2005). Continuous culture—Making a comeback? *Microbiology*, 151(10), 3153–3159.
- Huisman, O., D'Ari, R., & Gottesman, S. (1984). Cell-division control in *Escherichia coli*: Specific induction of the SOS function SfiA protein is sufficient to block septation. *Proceedings of the National Academy of Sciences*, 81(14), 4490–4494.
- Joers, A., Kaldalu, N., & Tenson, T. (2010). The frequency of persisters in *Escherichia coli* reflects the kinetics of awakening from dormancy. *Journal of Bacteriology*, 192(13), 3379–3384.
- Kim, M., Rai, N., Zorraquino, V., Tagkopoulos, I. (2016). Multi-omics integration accurately predicts cellular state in unexplored conditions for *Escherichia coli*. *Nature Communications*, 7, 13090.
- Kim, M., Tagkopoulos, I. (2018). Data integration and predictive modeling methods for multi-omics datasets. *Molecular Omics*, 14(1), 8–25.
- Kim, M., Zorraquino, V., Tagkopoulos, I. (2015). Microbial forensics: Predicting phenotypic characteristics and environmental conditions from large-scale gene expression profiles. *PLoS Computational Biology*, 11(3), e1004127.
- Lin, E. C. C. (1976). Glycerol dissimilation and its regulation in bacteria. *Annual Reviews in Microbiology*, 30(1), 535–578.
- López-García, P., & Forterre, P. (2000). DNA topology and the thermal stress response, a tale from mesophiles and hyperthermophiles. *BioEssays*, 22(8), 738–746.
- López-Maury, L., Marguerat, S., & Bähler, J. (2008). Tuning gene expression to changing environments: From rapid responses to evolutionary adaptation. *Nature Reviews Genetics*, 9(8), 583–593.
- Madan, R., Moorthy, S., & Mahadevan, S. (2008). Enhanced expression of the *bgl* operon of *Escherichia coli* in the stationary phase. *FEMS Microbiology Letters*, 288(1), 131–139.
- Manas, P., & Mackey, B. M. (2004). Morphological and physiological changes induced by high hydrostatic pressure in exponential- and stationary-phase cells of *Escherichia coli*: Relationship with cell death. *Applied and Environmental Microbiology*, 70(3), 1545–1554.
- Masse, E., & Gottesman, S. (2002). A small RNA regulates the expression of genes involved in iron metabolism in *Escherichia coli*. *Proceedings of the National Academy of Sciences*, 99(7), 4620–4625.
- Maurer, L. M., Yohannes, E., Bondurant, S. S., Radmacher, M., & Slonczewski, J. L. (2005). pH regulates genes for flagellar motility, catabolism, and oxidative stress in *Escherichia coli* K-12. *Journal of Bacteriology*, 187(1), 304–319.
- McKenzie, G. J., Harris, R. S., Lee, P. L., & Rosenberg, S. M. (2000). The SOS response regulates adaptive mutation. *Proceedings of the National Academy of Sciences*, 97(12), 6646–6651.
- Mozhayskiy, V., & Tagkopoulos, I. (2012). Horizontal gene transfer dynamics and distribution of fitness effects during microbial in silico evolution. *BMC Bioinformatics*, 13(10), S13.
- Mozhayskiy, V., Tagkopoulos, I. (2013). Microbial evolution in vivo and in silico: methods and applications. *Integrative Biology*, 5(2), 262–277.
- Nikel, P. I., Romero-Campero, F. J., Zeidman, J. A., Goñi-Moreno, Á., & de Lorenzo, V. (2015). The glycerol-dependent metabolic persistence of *Pseudomonas putida* KT2440 reflects the regulatory logic of the *GlpR* repressor. *mBio*, 6(2), e00340–15.
- Nobelmann, B., & Lengeler, J. W. (1996). Molecular analysis of the *gat* genes from *Escherichia coli* and of their roles in galactitol transport and metabolism. *Journal of Bacteriology*, 178(23), 6790–6795.
- Ochman, H., Lawrence, J. G., & Groisman, E. A. (2000). Lateral gene transfer and the nature of bacterial innovation. *Nature*, 405(6784), 299–304.
- Ohmori, H., Saito, M., Yasuda, T., Nagata, T., Fujii, T., Wachi, M., & Nagai, K. (1995). The *pcsA* gene is identical to *dinD* in *Escherichia coli*. *Journal of Bacteriology*, 177(1), 156–165.
- Österberg, S., Peso-Santos, T., & Shingler, V. (2011). Regulation of alternative sigma factor use. *Annual Review of Microbiology*, 65, 37–55.
- Rai, N., Rai, R., & Venkatesh, K. (2015). Quorum sensing in competence and sporulation, *Quorum sensing vs quorum quenching: a battle with no end in sight* (pp.61–64). India: Springer.
- Raivio, T. L. (2005). Envelope stress responses and Gram-negative bacterial pathogenesis. *Molecular Microbiology*, 56(5), 1119–1128.
- Rossouw, D., & Bauer, F. F. (2009). Comparing the transcriptomes of wine yeast strains: Toward understanding the interaction between environment and transcriptome during fermentation. *Applied Microbiology and Biotechnology*, 84(5), 937–954.
- Roy, S. W. (2016). Is mutation random or targeted?: No evidence for hypermutability in snail toxin genes. *Molecular Biology and Evolution*, 33(10), 2642–2647.
- Sambrook, J., & Russell, D. W., et al. (2001). *Molecular cloning: A laboratory manual*. 2001. New York: Cold Spring Harbor Laboratory Press.
- Sandberg, T. E., Pedersen, M., LaCroix, R. A., Ebrahim, A., Bonde, M., Herrgard, M. J., ... Feist, A. M. (2014). Evolution of *Escherichia coli* to 42 C and subsequent genetic engineering reveals adaptive mechanisms and novel mutations. *Molecular Biology and Evolution*, 31(10), 2647–2662.
- Schweizer, H., Boos, W., & Larson, T. J. (1985). Repressor for the sn-glycerol-3-phosphate regulon of *Escherichia coli* K-12: Cloning of the *glpR* gene and identification of its product. *Journal of Bacteriology*, 161(2), 563–566.
- Sharp, S. J., Schaack, J., Cooley, L., Burke, D. J., & Soil, D. (1985). Structure and transcription of eukaryotic tRNA gene. *CRC Critical Reviews in Biochemistry*, 19(2), 107–144.
- Shiloach, J., & Fass, R. (2005). Growing *E. coli* to high cell density? A historical perspective on method development. *Biotechnology Advances*, 23(5), 345–357.
- Subramanian, A., Tamayo, P., Mootha, V. K., Mukherjee, S., Ebert, B. L., Gillette, M. A., ... Mesirov, J. P. (2005). Gene set enrichment analysis: A knowledge-based approach for interpreting genome-wide expression profiles. *Proceedings of the National Academy of Sciences*, 102(43), 15545–15550.
- Sugai, R., Shimizu, H., Nishiyama, K., & Tokuda, H. (2004). Overexpression of *gnsA*, a multicopy suppressor of the *secG* null mutation, increases acidic phospholipid contents by inhibiting phosphatidylethanolamine synthesis at low temperatures. *Journal of Bacteriology*, 186(17), 5968–5971.
- Tan, I. S., & Ramamurthi, K. S. (2014). Spore formation in *Bacillus subtilis*. *Environmental Microbiology Reports*, 6(3), 212–225.
- Taylor, T. B., Mulley, G., Dills, A. H., Alsohim, A. S., McGuffin, L. J., Studholme, D. J., ... Jackson, R. W. (2015). Evolutionary resurrection of flagellar motility via rewiring of the nitrogen regulation system. *Science*, 347(6225), 1014–1017.
- Toprak, E., Veres, A., Michel, J.-B., Chait, R., Hartl, D. L., & Kishony, R. (2012). Evolutionary paths to antibiotic resistance under dynamically sustained drug selection. *Nature Genetics*, 44(1), 101–105.
- Torrent, M., Chalancon, G., de Groot, N. S., Wuster, A., & Madan Babu, M. (2018). Cells alter their tRNA abundance to selectively regulate protein synthesis during stress conditions. *Science Signaling*, 11(546), eaat6409.
- Tran, K. T., Maeda, T., Sanchez-Torres, V., & Wood, T. K. (2015). Beneficial knockouts in *Escherichia coli* for producing hydrogen from glycerol. *Applied Microbiology and Biotechnology*, 99(6), 2573–2581.
- Vaiphei, S. T., Pandey, G., & Mukherjee, K. J. (2009). Kinetic studies of recombinant human interferon-gamma expression in continuous cultures of *E. coli*. *Journal of Industrial Microbiology & Biotechnology*, 36(12), 1453–1458.
- Velur Selvamani, R. S., Friehs, K., & Flaschel, E. (2014). Extracellular recombinant protein production under continuous culture conditions

- with *Escherichia coli* using an alternative plasmid selection mechanism. *Bioprocess and Biosystems Engineering*, 37(3), 401–413.
- Wang, X., Zorraquino, V., Kim, M., Tsoukalas, A., Tagkopoulos, I. (2018). Predicting the evolution of *Escherichia coli* by a data-driven approach. *Nature Communications*, 9(1), 3562.
- Wood, T. K., Knabel, S. J., & Kwan, B. W. (2013). Bacterial persister cell formation and dormancy. *Applied and Environmental Microbiology*, 79(23), 7116–7121.
- Wrande, M., Roth, J. R., & Hughes, D. (2008). Accumulation of mutants in “aging” bacterial colonies is due to growth under selection, not stress-induced mutagenesis. *Proceedings of the National Academy of Sciences*, 105(33), 11863–11868.
- Yang, B., Gerhardt, S. G., & Larson, T. J. (1997). Action at a distance for glpTQ transcription in *Escherichia coli* K-12. *Molecular Microbiology*, 24(3), 511–521.
- Ye, Y., Zhang, L., Hao, F., Zhang, J., Wang, Y., & Tang, H. (2012). Global metabolomic responses of *Escherichia coli* to heat stress. *Journal of Proteome Research*, 11(4), 2559–2566.
- Yona, A. H., Bloom-Ackermann, Z., Frumkin, I., Hanson-Smith, V., Charpak-Amikam, Y., Feng, Q., ... Pilpel, Y. (2013). tRNA genes rapidly change in evolution to meet novel translational demands. *eLife*, 2, e01339–e01339.
- Zhang, Q., Lambert, G., Liao, D., Kim, H., Robin, K., Tung, C., ... Austin, R. H. (2011). Acceleration of emergence of bacterial antibiotic resistance in connected microenvironments. *Science*, 333(6050), 1764–1767.
- Zhong, J., Xiao, C., Gu, W., Du, G., Sun, X., He, Q.-Y., & Zhang, G. (2015). Transfer RNAs mediate the rapid adaptation of *Escherichia coli* to oxidative stress. *PLOS Genetics*, 11(6), e1005302.
- Zorraquino, V., Kim, M., Rai, N., & Tagkopoulos, I. (2017). The genetic and transcriptional basis of short and long term adaptation across multiple stresses in *Escherichia coli*. *Molecular Biology and Evolution*, 34(3), 707–717.

SUPPORTING INFORMATION

Additional supporting information may be found online in the Supporting Information section at the end of the article.

How to cite this article: Rai N, Huynh L, Kim M, Tagkopoulos I. Population collapse and adaptive rescue during long-term chemostat fermentation. *Biotechnology and Bioengineering*. 2019;116:693–703. <https://doi.org/10.1002/bit.26898>